EPSILON-FREE CURVATURE METHODS FOR SLOW-FAST DYNAMICAL SYSTEMS

MORTEN BRØNS*‡, MATHIEU DESROCHES†§, AND MARTIN KRUPA†¶

1. Introduction. Many dynamical systems exhibit a slow-fast structure where a solution from some arbitrary initial condition rapidly relaxes toward some attracting invariant manifold where the dynamics progresses slowly. Determining such manifolds is of obvious importance. On one hand they provide a basic insight into the dynamics of the system, on the other hand they allow a reduction of dimension as the asymptotic dynamics of the system occurs on the invariant manifold only. If the dimension of the invariant manifold is sufficiently low, this reduction may result in substantial savings in computational costs. Similarly, repelling invariant manifolds may act as separatrices in the phase space and hence be key object in the organization of the dynamics.

For systems of singular perturbation form,

$$\dot{x} = f(x, y), \quad x \in R^n, \tag{1.1a}$$

$$\dot{y} = \varepsilon g(x, y), \quad y \in R^m, \tag{1.1b}$$

where ε is a small parameter, Fenichel theory [13, 19, 10] provides a very useful characterization of invariant manifolds which we briefly review here. The critical manifold M_0 (of dimension m) for the system Eqns. (1.1) is defined as the set of points fulfilling $f(x, y) = 0$. Assuming M_0 is locally normally hyperbolic, that is, the eigenvalues of $D_x f$ at the manifold are off the imaginary axis, there is an invariant manifold M_ε close to M_0 when ε is sufficiently small. The stability properties of M_ε are determined by the eigenvalues of $D_x f$, and an asymptotic expansion of the manifold in the form of a graph,

$$x = h_\varepsilon(y) = h_0(y) + \varepsilon h_1(y) + \varepsilon^2 h_2(y) + \cdots, \tag{1.2}$$

where h_0 represents the critical manifold, $f(h_0(y), y)) = 0$, can be obtained by solving a sequence of linear equations.

For the case of $n = 1$ i.e. one fast variable, Fenichel theory provides an invariant hypersurface. It is attracting if $\partial f/\partial x < 0$ and repelling if $\partial f/\partial x > 0$.

Many systems which exhibit a slow-fast dynamics do not, however, have the explicit singular perturbation structure given by Eqns. (1.1) as no obvious small parameter ε can be identified. Several methods to obtain approximate invariant manifolds for such systems have been developed. A very popular one is the Intrinsic Low-Dimensional Manifold (ILDM) technique [20] which has proved most useful in reducing large systems arising in chemistry, in particular models for combustion processes. In two-dimensional systems the inflection line, i.e. the locus of points where the curvature of trajectories vanishes, has been shown to provide a good approximation

*Department of Applied Mathematics and Computer Science, Technical University of Denmark, Matematiktorvet, Building 303 S, DK-2800 Kongens Lyngby, Denmark.

†INRIA Paris-Rocquencourt Research Centre, Domaine de Voluceau, Rocquencourt BP 105, 78153 Le Chesnay cedex, France.

‡mobr@dtu.dk

§mathieu.desroches@inria.fr

¶maciej.krupa@inria.fr

of invariant manifolds [21, 23, 9, 11]. A more general method based on higher curvatures to obtain an approximately invariant manifold of co-dimension 1 in arbitrary dimension has been proposed in [17] and [18].

The purpose of the present paper is to investigate and compare these reduction techniques focusing on the special case of a reduction of dimension by one, i.e. approximation of invariant hypersurfaces, primarily for systems of dimension two or three.

2. Intrinsic low-dimensional manifolds (ILDM) and intrinsic hypersurfaces (IH). We first briefly review the construction of intrinsic low-dimensional manifolds. Consider the N-dimensional system

$$\dot{x} = F(x), \quad x \in R^N. \tag{2.1}$$

Consider the generic case where the eigenvalues $\lambda_p(x), p = 1, \ldots, N$ of the Jacobian matrix $J(x) = DF(x)$ are all different such that there is a basis of eigenvectors $v_p(x)$ for the tangent space to R^N at x. For complex eigenvalues we use real and imaginary parts of an eigenvector as base vectors. Order the eigenvalues such that

$$\mathrm{Re}\lambda_1(x) \leq \mathrm{Re}\lambda_2(x) \leq \cdots \leq \mathrm{Re}\lambda_{N-1}(x) \leq \mathrm{Re}\lambda_N(x). \tag{2.2}$$

Equality occurs only for pairs of complex eigenvalues. For convenience, we suppress the x-dependence from now on. In the ILDM method it is assumed there is a spectral gap at, say, λ_k such that $\mathrm{Re}\lambda_k \ll \mathrm{Re}\lambda_{k+1}$, clearly dividing the eigenvalues into fast ones and slow ones. The ILDM is then defined as the manifold of dimension $N-k$ where the fast components of F in the eigenvector base vanish. In formulas, let V be the matrix where the eigenvectors are columns. Then F can be expanded in the eigenvector basis as

$$F = V\alpha \tag{2.3}$$

where $\alpha = (\alpha_1, \alpha_2, \ldots, \alpha_N)^T$. This yields

$$\alpha = V^{-1}F \tag{2.4}$$

and the ILDM is then defined from

$$\alpha_1 = \cdots = \alpha_k = 0. \tag{2.5}$$

In [19] it is shown that for a singular perturbation system of the form Eqns. (1.1) the ILDM of dimension m based on the spectral gap defined by ε agrees with the Fenichel manifold to order ε.

Note that manifolds of dimension $N-k$ can be formally constructed from Eqns. (2.5) independently of any spectral gap or the ordering of the eigenvalues. In particular, we can define a number of intrinsic hypersurfaces IH, one from each of the equations $\alpha_k = 0$ where λ_k is real.

The following theorem shows that the union of all IH can be found in a simple way.

THEOREM 1. *A point $x \in R^N$ belongs to some intrinsic hypersurface if and only if the $N \times N$ determinant*

$$\mathrm{MP} = \det[\ F \quad JF \quad J^2F \quad \cdots \quad J^{N-1}F\ ] \tag{2.6}$$

vanishes at x.

Proof. The columns of MP are

$$F = \sum_{p=1}^{N} \alpha_p v_p, \quad JF = \sum_{p=1}^{N} \alpha_p \lambda_p v_p, \quad \dots \quad J^{N-1}F = \sum_{p=1}^{N} \alpha_p \lambda_p^{N-1} v_p, \tag{2.7}$$

and MP $= 0$ if and only if these vectors are linearly dependent. This is the case exactly if the matrix A given by

$$A = \begin{bmatrix} \alpha_1 & \alpha_1\lambda_1 & \cdots & \alpha_1\lambda_1^{N-1} \\ \alpha_2 & \alpha_2\lambda_2 & \cdots & \alpha_2\lambda_2^{N-1} \\ \vdots & \vdots & \ddots & \vdots \\ \alpha_N & \alpha_N\lambda_N & \cdots & \alpha_n\lambda_n^{N-1} \end{bmatrix} \tag{2.8}$$

is singular. Since A can be written as a product of a diagonal matrix and a Vandermonde matrix,

$$A = \operatorname{diag}[\alpha_1, \alpha_2, \dots, \alpha_N] \begin{bmatrix} 1 & \lambda_1 & \cdots & \lambda_1^{N-1} \\ 1 & \lambda_2 & \cdots & \lambda_2^{N-1} \\ \vdots & \vdots & \ddots & \vdots \\ 1 & \lambda_N & \cdots & \lambda_N^{N-1} \end{bmatrix} \tag{2.9}$$

we have

$$\det A = \alpha_1\alpha_2\cdots\alpha_N \prod_{1\le k<l\le N} (\lambda_l - \lambda_k) \tag{2.10}$$

which is zero if and only if $\alpha_p = 0$ for some p. □

An intersection of some IHs will correspond to an ILDM of lower dimension, and hence such manifolds are contained in the solution set for MP $= 0$. However, they will only have a dynamical significance if they correspond to a choice of the equations $\alpha_p = 0$ where λ_p is a fast eigenvalue.

Note that Theorem 1 does not discuss the invariance of the sets defined by $\alpha_k = 0$ or MP $= 0$. However, in the case J is stationary, that is $\mathrm{d}J/\mathrm{d}t = 0$, it is shown in [18] that the set given by MP $= 0$ is invariant.

2.1. Two-dimensional dynamics. For $N = 2$ Eqn. (2.6) becomes

$$\mathrm{MP} = \det \begin{bmatrix} F & JF \end{bmatrix}. \tag{2.11}$$

Since

$$\dot{x} = F, \quad \ddot{x} = JF \tag{2.12}$$

we have

$$\mathrm{MP} = \det \begin{bmatrix} \dot{x} & \ddot{x} \end{bmatrix} = \kappa|\dot{x}|^3, \tag{2.13}$$

where κ is the (signed) curvature of the trajectory $x(t)$. Defining the inflection line for a two-dimensional system as the set of points where the curvature of the trajectories vanishes, we have

THEOREM 2. *The collection of intrinsic hypersurfaces is the inflection line.*

Let us briefly review this in the specific case of the van der Pol equation

$$\dot{x} = y - \Phi(x), \tag{2.14a}$$
$$\dot{y} = \varepsilon(c - x), \tag{2.14b}$$

where $\Phi(x) = x^3/3 - x$. More information can be found in [9, 17, 11]. In particular, §5.1 in [17] provides many details for the case $c = 0$.

The inflection line is easily found as

$$y_\pm(x) = \Phi(x) + \frac{c-x}{2}\left[\Phi'(x) \pm \sqrt{\Phi'(x)^2 - 4\varepsilon}\right]. \tag{2.15}$$

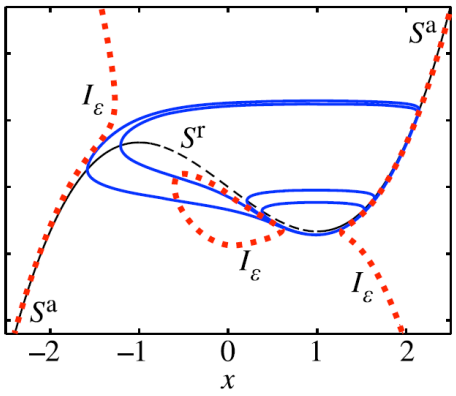

FIG. 2.1. *The van der Pol equation for $\varepsilon = 0.1$. Black curve: Critical manifold. Red curve: Inflection line for $c = 1$. Blue curves: Sample trajectories for c close to 1. From [11].*

It appears from Fig. 2.1 that the inflection line has several branches which meet in fold points and that some of the branches have a dynamical significance as they are good approximations to solution curves while others are not. This can be understood from the ILDM point of view. At any point in the phase space where there are real and different eigenvalues the functions α_1 and α_2 are defined from Eqn. (2.4). The equation $\alpha_1 = 0$ defines an ILDM, since here the fastest component of the vector field vanishes, and this constitutes the approximately invariant manifold. The other equation, $\alpha_2 = 0$, is the locus of points where the slowest component of the velocity field vanishes, and this is not expected to be approximately invariant. The manifolds defined by an incorrect identification of fast and slow directions have been denoted "ghost manifolds" in [4, 5]. The fold point of the inflection line is where there is a double eigenvalue. This marks the boundary to a region with complex eigenvalues where the is no spectral gap and hence the α_k cannot be defined.

3. Higher curvature hypersurfaces (HCH). In a series of papers [17, 18, 15, 16] Jean-Marc Ginoux and co-workers have proposed to study the zero set of the $N \times N$ determinant

$$\mathrm{G} = \det\left[\dot{x} \quad \ddot{x} \quad \ldots \quad \overset{(N-1)}{x}\right] \tag{3.1}$$

as approximations of slow invariant manifolds for systems (2.1). The geometric interpretation is that the set $\mathrm{G} = 0$ is the locus of points where the (higher) curvature of the trajectories is zero. For $N = 2$ the higher curvature is simply classical curvature,

for $N = 3$ it is torsion, and so on. In the present paper we will denote the surfaces $\mathrm{G} = 0$ *higher curvature hypersurfaces* (HCH).

In the special case of a stationary Jacobian, G = MP; Hence, as discussed in §2 the surface $\mathrm{G} = 0$ is invariant [18].

By differentiation of Eq. (2.1) one finds

$$\ddot{x} = JF, \quad \dddot{x} = (D^2F)F^2 + J^2F \tag{3.2}$$

which shows that for $N = 2$ we have in general G = MP but for $N = 3$ they differ since

$$\mathrm{G} = \mathrm{MP} + \det \begin{bmatrix} F & JF & (D^2F)F^2 \end{bmatrix}, \tag{3.3}$$

and consequently $\mathrm{G} \neq \mathrm{MP}$ for $N \geq 3$.

For systems on singular perturbation form (1.1) with $n = 1$ and $N = m + 1$ one can try to obtain an asymptotic expansion of a solution of $\mathrm{G} = 0$ close to the critical manifold on the form

$$x = h_0(y) + \epsilon H_1(y) + \epsilon^2 H_2(y) + \cdots . \tag{3.4}$$

Ginoux ([18], see also [14], in particular §11.3 and proposition 11.3) state that the agreement between the expansion (3.4) and the expansion (1.2) of the Fenichel manifold depends on the dimension N of the system. Specifically, $H_k = h_k$ for $k < N$. For more details on the non-degeneracy conditions needed for this result to hold, and for results on approximation of Fenichel manifolds by zero sets of other tests functions than MP and G, see [1]. Here we focus on the fact that the set $\mathrm{G} = 0$ can be determined for slow-fast systems which are not on singular perturbation form and we can enhance the accuracy of the approximation to the Fenichel manifold which is obtained in this way by increasing the dimension of the system. We now demonstrate this for $N = 2$, using direct computations with Maple, as an alternative to the arguments of Ginoux, based on differential geometry.

We first add a single slow equation, $\dot{z} = \delta z, \delta \ll 1$ to the system (2.1). This yields for the augmented system

$$\mathrm{G} = \det \begin{bmatrix} \dot{x} & \ddot{x} & \dddot{x} \\ \delta z & \delta^2 z & \delta^3 z \end{bmatrix} = \delta \det \begin{bmatrix} \ddot{x} & \dddot{x} \end{bmatrix} + O(\delta^2) \tag{3.5}$$

which suggests to consider the zero set for the function

$$\mathrm{G}_{23} = \det \begin{pmatrix} \ddot{x} & \dddot{x} \end{pmatrix}. \tag{3.6}$$

For a singular perturbation system

$$\dot{x} = f(x, y), \quad x \in R, \tag{3.7a}$$
$$\dot{y} = \varepsilon g(x, y), \quad y \in R, \tag{3.7b}$$

we can show, using the symbolic program Maple, that an expansion of the form (3.4) generically agrees with the Fenichel manifold to order ϵ^2.

This result can be improved by adding two equations, $\dot{z}_1 = \delta z_1, \dot{z}_2 = a\delta z_2$ for $\delta \ll 1$ and a fixed. Note that we need all eigenvalues to be different and therefore must have $a \neq 1$. This gives

$$\mathrm{G} = \det \begin{bmatrix} \dot{x} & \ddot{x} & \dddot{x} & \ddddot{x} \\ \delta z_1 & \delta^2 z_1 & \delta^3 z_1 & \delta^4 z_1 \\ a\delta z_2 & a\delta^2 z_2 & a\delta^3 z_2 & a\delta^4 z_2 \end{bmatrix} = \delta^3 a(a-1) z_1 z_2 \det \begin{bmatrix} \dddot{x} & \ddddot{x} \end{bmatrix} + O(\delta^4) \tag{3.8}$$

Base function	accuracy	Derived function	accuracy
$\mathrm{G} = \det\begin{bmatrix}\dot{x} & \ddot{x}\end{bmatrix}$	ε^1	$\mathrm{G}_{13} = \dfrac{\mathrm{d}G}{\mathrm{d}t} = \det\begin{bmatrix}\dot{x} & \dddot{x}\end{bmatrix}$	ε^2
$\mathrm{G}_{23} = \det\begin{bmatrix}\ddot{x} & \dddot{x}\end{bmatrix}$	ε^2	$\mathrm{G}_{24} = \dfrac{\mathrm{d}G_{23}}{\mathrm{d}t} = \det\begin{bmatrix}\ddot{x} & \ddddot{x}\end{bmatrix}$	ε^3
$\mathrm{G}_{13} = \det\begin{bmatrix}\dot{x} & \dddot{x}\end{bmatrix}$	ε^2	$\mathrm{G}_{2314} = \dfrac{\mathrm{d}G_{13}}{\mathrm{d}t} = \det\begin{bmatrix}\ddot{x} & \dddot{x}\end{bmatrix} + \det\begin{bmatrix}\dot{x} & \ddddot{x}\end{bmatrix}$	ε^3

TABLE 3.1

Obtaining new functions by differentiation in two-dimensional systems. For each function, the order to which the zero set agrees with the Fenichel manifold for the singular perturbation system Eqns. (3.7) is shown.

which leads to the definition

$$\mathrm{G}_{34} = \det\begin{bmatrix}\dddot{x} & \ddddot{x}\end{bmatrix} \tag{3.9}$$

for which we find, again using Maple, that we can generically obtain an approximation to the Fenichel manifold accurate to order ϵ^3.

An alternative approach to increasing the accuracy of the approximation of the invariant manifold is by the zero-derivative principle [24, 25], the idea being that if a function is approximately conserved under the dynamics the zero set of its time derivative defines an even more accurate approximation of the slow manifold.

Table 3.1 shows a list of quantities generated in this way for a two-dimensional system. In all cases the accuracy of the approximation of the Fenichel manifold for the system (2.14) increases by one order. This result is obtained by symbolic computations in Maple and holds under generic non-degeneracy conditions.

4. Extending invariant manifolds across folds of the critical manifold.

4.1. The van der Pol equation. We show in Fig. 4.1 some specific examples for the van der Pol equation (2.14) of the approximately invariant manifolds described in the previous section.

On the attracting sides of the critical manifold, the proposed manifolds all follow the stable limit cycle closely until a fold is reached. For $c = 0.8$ there is an unstable fixed point on the critical manifold at $x = 0.8$. The repelling Fenichel manifold passes through that point. To the left of the fixed point all manifolds approximate the Fenichel manifold very well. It is interesting to note that the manifold $\mathrm{G}_{23} = 0$ is qualitatively different from the others since it has the surprising property that it is well-defined at the fold point $x = 1$; the Fenichel manifold and $\mathrm{G}_{24} = 0$ have vertical asymptotes here. For $c = 0.99$ we essentially see the same picture. However, the limit cycle stays close to the repelling invariant manifold for $x < 1$ for a while and is then a canard trajectory [2, 26]. A minor change to $c = 1.01$ shows that the repelling Fenichel manifold (defined as such for $-1 < x < 1$) and the attracting Fenichel manifold (defined as such for $x > 1$) have changed their relative position. Likewise, the asymptotic behavior of the first-order approximation to the Fenichel manifold and the $\mathrm{G}_{24} = 0$ manifold has changed. The value of c where the two Fenichel manifolds agree is the canard point c_c. It marks the center of the transition from small to large limit cycles, the canard explosion, as c is varied. The asymptotic expansion is

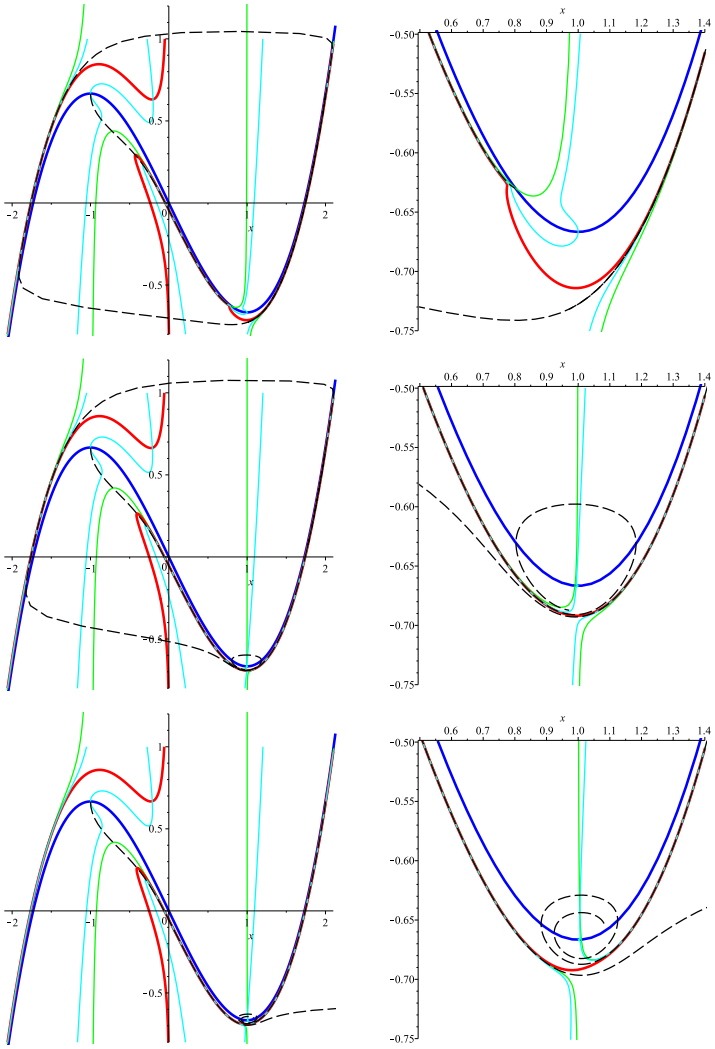

FIG. 4.1. *Manifolds and numerical solutions for the van der Pol equation, $\varepsilon = 0.05$. Top row: $c = 0.8$. Middle row: $c = 0.99$. Bottom row: $c = 1.01$ The right panels show details near the fold of the critical manifold at $x = 1$. Blue curve: critical manifold. Lower black dashed curve: limit cycle. Upper black dashed curve: Repelling Fenichel manifold obtained by backward integration starting from the maximum of the critical manifold. Green curve: First-order approximation to Fenichel manifold. Red curve:* $\mathrm{G}_{23} = 0$. *Cyan curve:* $\mathrm{G}_{24} = 0$.

well-defined, and for the van der Pol equation one finds

$$c_c = 1 - \frac{1}{8}\varepsilon - \frac{3}{32}\varepsilon^2 + O(\varepsilon^3) \tag{4.1}$$

see e.g. [26, 6]. This is obtained by inserting a Poincaré-Lindstedt expansion of the Fenichel manifold in the equation for the trajectories obtained from Eqns. (2.14),

$$y = f(x) + y_1(x)\varepsilon + y_2(x)\varepsilon^2 + \cdots, \quad c = c_0 + c_1\varepsilon + c_2\varepsilon^2 + \cdots, \tag{4.2}$$

and requiring that each y_k does not have a singularity at the fold of the critical manifold.

Fig. 4.1 indicates that a similar approach could be used to obtain the canard point from G_{24}. We do this by solving

$$G_{24} = 0, \quad \frac{\partial G_{24}}{\partial x} = 0, \quad \frac{\partial G_{24}}{\partial y} = 0 \tag{4.3}$$

for x, y, c. For the van der Pol equation with $\varepsilon = 0.05$ this yields

$$c = 0.993628, \quad x = 0.991437, \quad y = -.691947. \tag{4.4}$$

The corresponding manifold manifold, shown in Fig. 4.2, has a double point, in agreement with the conditions Eqns. (4.3), and the configurations in the two lower rows of Fig. 4.1 are unfoldings hereof. A very good agreement with the asymptotic value $c_c = 0.993515$ from Eqn. (4.1) is obtained.

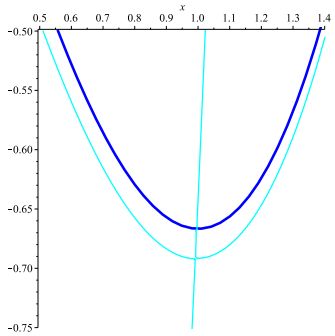

FIG. 4.2. *Canard manifold for the van der Pol equation. Blue curve: Critical manifold. Cyan curve: The manifold $G_{24} = 0$ for the canard point c given by Eqn. (4.4).*

This agreement is no coincidence. Inserting an expansion Eqn. (4.2) in $G_{24} = 0$, solving for y_k and choosing c_{k-1} such that zeroes in the numerator and the denominator cancel, yields Eqn. (4.1) to second order accuracy. In more generality, we have that the ε^k-accurate methods allow a determination of the canard point to accuracy ε^{k-1}.

4.2. The Templator. The results in the previous sections provide ε-free methods to determine canard points in two-dimensional systems. We demonstrate here that G_{23} can be used for this purpose on a slow-fast system with no distinguished small parameter. We consider the Templator

$$\frac{dX}{dt} = r - k_u X^2 - k_T X^2 T, \tag{4.5a}$$

$$\frac{dT}{dt} = k_u X^2 + k_T X^2 T - \frac{qT}{K+T} \tag{4.5b}$$

which is a simple model of an autocatalytic process where the species T act as template for its own creation. For further details on the chemistry behind the model see [22, 3] and references therein. Considering the inflow rate r as a parameter, the system has two canard explosions, first noted in [3], see Fig. 4.3.

Numerically, two canard explosions are found at $r = 0.4199$ and $r = 0.9676$. Solving Eqns. (4.3) for this system numerically yields $r = 0.4198$ and $r = 0.9675$ in very good agreement with the results from numerical simulations. These canard

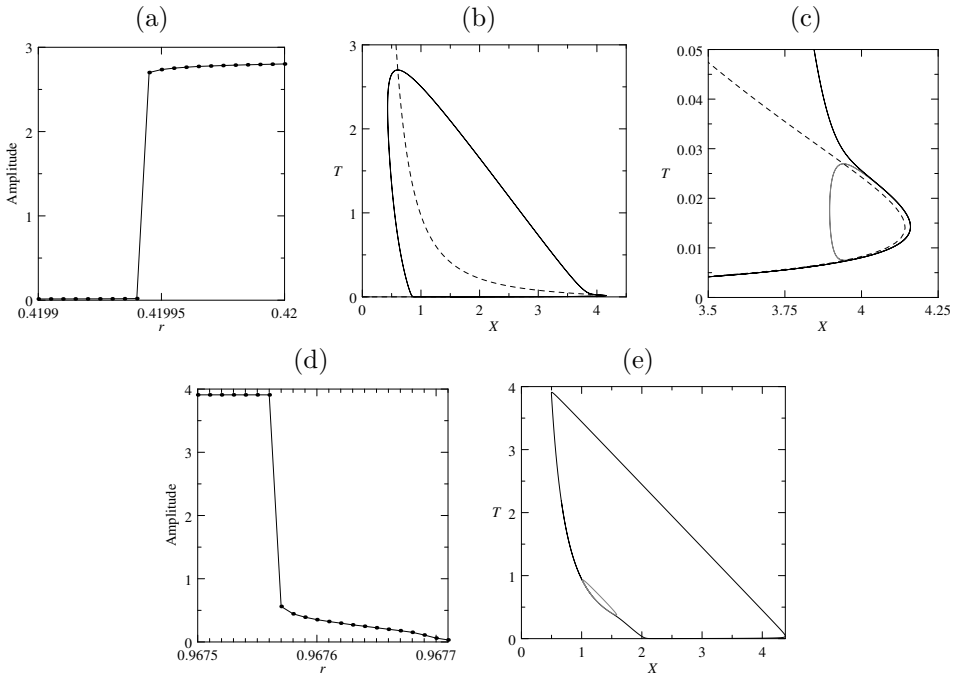

FIG. 4.3. *Canard explosion in the Templator, Eqns.* (4.5) *for* $k_u = 0.01, k_T = 1, K = 0.02, q = 1$. *(a): Bifurcation diagram for low* r *(b): The large limit cycle after the explosion. The dashed line is the critical manifold found by an asymptotic analysis. (c): Detail showing the small limit cycle (gray) before the explosion. (d): Bifurcation diagram for high* r*. (e): Limit cycles before/after (black/gray) the explosion. From [7].*

points has also been found analytically in [7] by identifying two different scalings which allow the introduction of a small parameter and in [8] using an iterative method. The present method is clearly the most simple and direct one.

5. The inflection line method in 2D and 3D canard problems.

5.1. Inflection lines in "canard explosive systems". The idea of inflection has regularly emerged and disappeared in the analysis of multiple time scale systems over the last four decades. It seems to date back (at least) to the work of M. Okuda [21] at the end of the 1970s, already in link with excitability but not yet with canards. At the beginning of the 1990s, in [23], Peng *et al.* applied it to canard explosive systems in the context of chemical reactions, showing that some component of the inflection set associated with a planar slow-fast system could allow to separate, in a loose sense, headless canards from canards with head. They stated an erroneous result about the possibility for discontinuous canard explosions, which was corrected a few years later by M. Brøns and K. Bar-Eli ([9]), still in a chemical context. Aside the work of Ginoux, using a very similar idea to compute implicit equations for slow manifolds away from non-hyperbolic regions of the unperturbed system, the most recent use of the inflection line method is due to Desroches and coauthors [11, 12]).

5.2. Inflection lines in "folded node systems".

5.2.1. The minimal folded node system as a planar non-autonomous system. Here we try to use the idea of inflection lines of the flow to a minimal three-

dimensional system displaying a *folded node*. The basic mechanism for folded node dynamics, which generates small oscillations — which may become SAOs of possible MMOs provided a suitable return mechanism is added to this minimal system — near the fold of a two-dimensional critical manifold, is to put a slow dynamics on parameter unfolding a *canard explosion* in a planar slow-fast system. The simplest slow dynamics is given by a constant slow drift, which makes the minimal folded node type system look like the following one

$$x' = -y + x^2 - x^3 \tag{5.1}$$
$$y' = \varepsilon(z + x) \tag{5.2}$$
$$z' = \varepsilon\mu, \tag{5.3}$$

with $0 < \varepsilon, \mu \ll 1$. System (5.1)–(5.3) is actually of dimension "two and a half" in the sense that it can be written as a planar *non-autonomous* system as below

$$x' = -y + x^2 - x^3 \tag{5.4}$$
$$y' = \varepsilon(\varepsilon\mu t + z_0) \tag{5.5}$$

Now we can try to apply the inflection line method to the non-autonomous planar system (5.4)–(5.5). We first write the trajectory equation

$$\frac{dy}{dx} = \frac{\varepsilon(\varepsilon\mu t + z_0 + x)}{-y + x^2 - x^3}, \tag{5.6}$$

which we can re-write in the form

$$(-y + x^2 - x^3)\frac{dy}{dx} - \varepsilon(\varepsilon\mu t + z_0) - \varepsilon x = 0. \tag{5.7}$$

Equation (5.7) can be differentiated with respect to x with the inflection condition $y''(x) = 0$ being plugged in; the difference with the usual case is the presence of t which must then also be differentiated with respect to x, giving

$$-\left(\frac{dy}{dx}\right)^2 + (2x - 3x^2)\frac{dy}{dx} - \varepsilon^2\mu\frac{dt}{dx} - \varepsilon = 0, \tag{5.8}$$

with $\frac{dy}{dx} = \frac{\varepsilon(\varepsilon\mu t + z_0 + x)}{h}$ and $\frac{dt}{dx} = \frac{1}{h}$, and with $h = -y + x^2 - x^3$. Therefore, equation (5.8) becomes

$$-\frac{\varepsilon^2(\varepsilon\mu t + z_0 + x)^2}{h^2} + (2x - 3x^2)\frac{\varepsilon(\varepsilon\mu t + z_0 + x)}{h} - \varepsilon^2\mu\frac{1}{h} - \varepsilon = 0. \tag{5.9}$$

Rearranging and simplifying gives, we finally obtain the t-dependent quadratic inflection equation

$$h^2 + \left(\varepsilon\mu - (2x - 3x^2)(\varepsilon\mu t + z_0 + x)\right)h + \varepsilon(\varepsilon\mu t + z_0 + x)^2 = 0. \tag{5.10}$$

The general solution of equation (5.10) is given by

$$h_\pm(x) = \frac{1}{2}\left(-\varepsilon\mu + (2x - 3x^2)(\varepsilon\mu t + z_0 + x) \pm \sqrt{\Delta}\right), \tag{5.11}$$

with

$$\Delta = \left[\varepsilon\mu - (2x - 3x^2)(\varepsilon\mu t + z_0 + x)\right]^2 - 4\varepsilon\left(\varepsilon\mu t + z_0 + x\right)^2. \tag{5.12}$$

5.2.2. Extracting information about ε and μ from the inflection line. From our previous work on inflection sets, we could characterise their topological shapes by rewriting the inflection equation as a *bifurcation problem with a distinguished parameter* and using the classification provided in the book by Golubitsky and Schaeffer. One can do the same for the inflection equation associated with folded node systems. To get more information about the relationship between inflection sets and the dynamics near a folded node, it is useful to evaluate the inflection equation close to the folded node and for a "time frame" corresponding to it, that is, for $|x-2/3| < \varepsilon$ and for $\varepsilon\mu t + z_0 = z_{\mathbf{fn}} = -2/3$, where $z_{\mathbf{fn}}$ is the z-coordinate of the folded node. In these conditions, the inflection equation (5.10) gets the following simplified form

$$h^2 + \left[\varepsilon\mu - (2x - 3x^2)\left(-\frac{2}{3} + x\right)\right] h + \varepsilon\left(-\frac{2}{3} + x\right)^2 = 0. \tag{5.13}$$

Then, completing the square in (5.13) yields

$$\bar{h}^2 - \frac{1}{4}\left[\varepsilon\mu - (2x - 3x^2)\left(-\frac{2}{3} + x\right)\right]^2 + \varepsilon\left(-\frac{2}{3} + x\right)^2 = 0, \tag{5.14}$$

with

$$\bar{h} = h + \frac{1}{2}\left[\varepsilon\mu - (2x - 3x^2)\left(-\frac{2}{3} + x\right)\right]. \tag{5.15}$$

This can be conveniently rewritten in the following way

$$\bar{h}^2 - \left(\sqrt{\frac{\varepsilon\mu}{2}}\right)^4 + \left(\left(-\frac{2}{3} + x\right)(\varepsilon - \frac{1}{4}(2x - 3x^2)^2)\right) + \left(\sqrt{\frac{\varepsilon\mu}{2}}\right)^2 (2x - 3x^2)\left(-\frac{2}{3} + x\right) = 0. \tag{5.16}$$

Now equation (5.16) can be recasted as a bifurcation problem with a distinguished parameter, and it can be written in the form of case 8^- on page 208 of Golubitsky & Schaeffer, Volume 1, that is

$$X^2 - \lambda^4 + \alpha + \beta\lambda + \gamma\lambda^2, \tag{5.17}$$

with

$$X = \bar{h}, \tag{5.18}$$

$$\lambda = \sqrt{\frac{\varepsilon\mu}{2}}, \tag{5.19}$$

$$\alpha = \left(\left(-\frac{2}{3} + x\right)(\varepsilon - \frac{1}{4}(2x - 3x^2)^2)\right), \tag{5.20}$$

$$\beta = 0, \tag{5.21}$$

$$\gamma = (2x - 3x^2)\left(-\frac{2}{3} + x\right). \tag{5.22}$$

The shape of the solution to equation (5.17) is shown on figure 5.1. This shows that when $\mu > 0$, that is, in the folded node case, an additional closed component of

the inflection line exists, contrary to the planar case where only one point of this "bubble" exists (the equilibrium point). We can now show, using simple asymptotic expansions in μ of the solutions to the equation $\Delta = 0$, where Δ is the discriminant of the (quadratic) inflection equation, that the maximal diameter of this small ellipse is of order $\sqrt{\varepsilon}\mu$.
Indeed, the fold points of the inflection set with respect to the vertical axis correspond to zeroes of the discriminant of the inflection equation, that is, the solutions to equation (5.12). In the time frame corresponding to the folded node, the equation $\Delta = 0$ reduces to

$$(2x - 3x^2)\left(-\frac{2}{3} + x\right) - \varepsilon\mu = \pm 2\sqrt{\varepsilon}\left(-\frac{2}{3} + x\right). \tag{5.23}$$

Expanding the solution to first order in μ, that is, writing $x = x_0 + x_1\mu + o(\mu^2)$, gives

$$\begin{aligned}(2x_0 - 3x_0^2)\left(-\frac{2}{3} + x_0\right) \\ + x_1\left(2\left(-\frac{2}{3} + x_0\right) + 3(2x_0 - 3x_0^2)\right)\mu - \varepsilon\mu + o(\mu^2) \\ = \pm 2\sqrt{\varepsilon}\left(-\frac{2}{3} + x_0 + x_1\mu\right) + o(\mu^2).\end{aligned} \tag{5.24}$$

Now collecting the terms of same order in μ on both sides of equation (5.24) provides the following expressions for x_0 and x_1 in terms of ε

$$(2x_0 - 3x_0^2)\left(-\frac{2}{3} + x_0\right) = \pm 2\sqrt{\varepsilon}\left(-\frac{2}{3} + x_0\right), \tag{5.25}$$

$$x_1\left(2\left(-\frac{2}{3} + x_0\right) + 3(2x_0 - 3x_0^2)\right) - \varepsilon = \pm 2\sqrt{\varepsilon}x_1. \tag{5.26}$$

Equation (5.25) is the unperturbed equation, that is, for $\mu = 0$, and its solutions are

$$x_0 = \frac{2}{3}, \quad x_0 = \frac{1}{3}\left(1 \pm \sqrt{1 \mp 6\sqrt{\varepsilon}}\right). \tag{5.27}$$

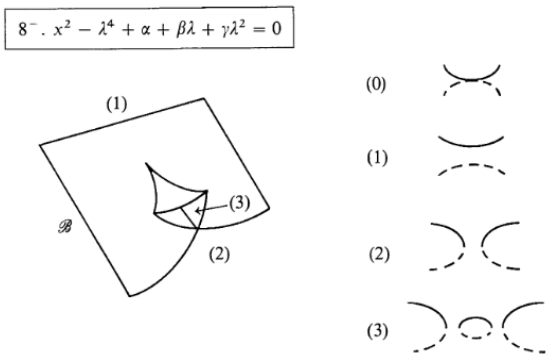

FIG. 5.1. *extracted from Golubitsky & Schaeffer vol. 1, page 208.*

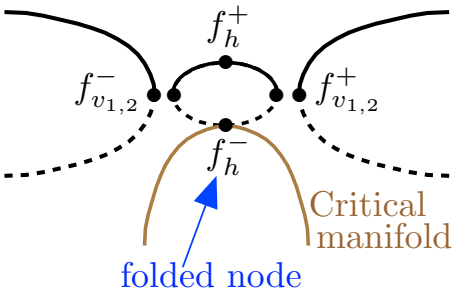

FIG. 5.2. *Configuration of the inflection set for the folded node minimal system (5.1)–(5.3), evaluated at the time frame that corresponds to the folded node, that is, for $\mu > 0$. The coordinates of the fold points $f_{v,h}^{\pm}$ can be estimated using basic expansions in μ.*

Evaluating equation (5.26) for these values of x_0 gives

$$x_1 = \pm\frac{\sqrt{\varepsilon}}{2}. \tag{5.28}$$

Finally, the solutions to the equation $\Delta = 0$ evaluated at the time-frame corresponding to the folded node are

$$x = x_0 \pm \frac{\sqrt{\varepsilon}}{2}\mu + o(\mu^2), \tag{5.29}$$

where x_0 is given by the formulas (5.27). This gives the coordinates of the vertical fold points, $f_v^{\pm}$, of the small ellipse component of the inflection set; see figure 5.2. From the above analysis we can deduce that the x-coordinates of the vertical fold points $f_v^{\pm}$ are given by

$$f_{v,x}^{\pm} = \frac{2}{3} \pm \frac{\sqrt{\varepsilon}}{2}\mu + o(\mu^2). \tag{5.30}$$

Furthermore, the horizontal fold points $f_h^{\pm}$ have an x-coordinate equal to $2/3$ and their y-coordinates are given by $4/27 + \varepsilon\mu$ and $4/27$, respectively. This is easily obtained by evaluating the inflection equation corresponding the folded node time frame at $x = 2/3$, which reduces to

$$h^2 + \varepsilon\mu h = 0, \tag{5.31}$$

whose solutions are $h = 0$ — that is, the upper fold point of the critical manifold C^0, see figure 5.2 below — and $h = -\varepsilon\mu$. Consequently, we have

$$f_h^- = \left(\frac{2}{3}, \frac{4}{27}\right), \tag{5.32}$$

$$f_h^+ = \left(\frac{2}{3}, \frac{4}{27} + \varepsilon\mu\right). \tag{5.33}$$

This analysis reveals that one can extract information about μ and ε by the sole knowledge of the inflection set; moreover, both of these key parameters can be independently. Indeed, although the above formulas contain the factor $\varepsilon\mu$ as a block, one can recover ε from the distance between the fold points of the inflection set near the lower fold of the critical manifold, which falls out of the analysis already done in the planar (canard explosion) case.

REFERENCES

[1] E. Benoit, M. Brøns, M. Desroches, and M. Krupa, *Extending the zero-derivative principle for slow-fast dynamical systems*. In preparation, 2014.

[2] E. Benoit, J. L. Callot, F. Diener, and M. Diener, *Chasse au canard*, Collectanea Mathematica, 32 (1981), pp. 37–119.

[3] K. M. Beutel and E. Peacock-López, *Complex dynamics in a cross-catalytic self-replication mechanism*, Journal of Chemical Physics, (2010).

[4] S. Borok, I. Goldfarb, and V. Gol'dshtein, *About non-coincidence of invariant manifolds and intrinsic low dimensional manifolds (ILDM)*, Communications in Nonlinear Science and Numerical Simulation, 13 (2008), pp. 1029–1038.

[5] ———, *Causes for "ghost" manifolds*, Communications in Nonlinear Science and Numerical Simulation, 14 (2009), pp. 1791–1795.

[6] M. Brøns, *Relaxation oscillations and canards in a nonlinear model of discontinuous plastic deformation in metals at very low temperatures*, Proceedings of the Royal Society of London. Series A: Mathematical, Physical and Engineering Sciences, 461 (2005), p. 2289–2302.

[7] ———, *Canard explosion of limit cycles in templator models of self-replication mechanisms*, The Journal of Chemical Physics, 134 (2011), pp. 144105–144105–5.

[8] Morten Brøns, *An iterative method for the canard explosion in general planar systems*, arXiv:1209.1109, (2012).

[9] Morten Brøns and Kedma Bar-Eli, *Asymptotic analysis of canards in the EOE equations and the role of the inflection line*, Proceedings of the Royal Society of London. Series A: Mathematical, Physical and Engineering Sciences, 445 (1994), pp. 305–322.

[10] Mathieu Desroches, John Guckenheimer, Bernd Krauskopf, Christian Kuehn, Hinke M. Osinga, and Martin Wechselberger, *Mixed-mode oscillations with multiple time scales*, SIAM Review, 54 (2012), pp. 211–288.

[11] Mathieu Desroches and Mike R. Jeffrey, *Canards and curvature: the 'smallness of ε' in slow–fast dynamics*, Proceedings of the Royal Society A: Mathematical, Physical and Engineering Sciences, 467 (2011), pp. 2404–2421.

[12] Mathieu Desroches, Martin Krupa, and Serafim Rodrigues, *Inflection, canards and excitability threshold in neuronal models*, Journal of Mathematical Biology, (in press) (2012).

[13] Neil Fenichel, *Geometric singular perturbation theory for ordinary differential equations*, Journal of Differential Equations, 31 (1979), pp. 53–98.

[14] Jean-Marc Ginoux, *Differential geometry applied to dynamical systems*, World Scientific, 2009.

[15] Jean-Marc Ginoux and Jaume Llibre, *The flow curvature method applied to canard explosion*, Journal of Physics A: Mathematical and Theoretical, 44 (2011), p. 465203.

[16] Jean-Marc Ginoux, Jaume Llibre, and Leon O. Chua, *Canards from Chua's circuit*, International Journal of Bifurcation and Chaos, 23 (2013), p. 1330010.

[17] Jean-Marc Ginoux and Bruno Rossetto, *Differential geometry and mechanics: applications to chaotic dynamical systems*, International Journal of Bifurcation and Chaos, 16 (2006), pp. 887–910.

[18] Jean-Marc Ginoux, Bruno Rossetto, and Leon O. Chua, *Slow invariant manifolds as curvature of the flow of dynamical systems*, International Journal of Bifurcation and Chaos, 18 (2008), pp. 3409–3430.

[19] Hans G. Kaper and Tasso J. Kaper, *Asymptotic analysis of two reduction methods for systems of chemical reactions*, Physica D: Nonlinear Phenomena, 165 (2002), pp. 66–93.

[20] U. Maas and S. B. Pope, *Simplifying chemical kinetics: Intrinsic low-dimensional manifolds in composition space*, Combustion and Flame, 88 (1992), pp. 239–264.

[21] M. Okuda, *Inflector analysis of the second stage of the transient phase for an enzymatic one-substrate reaction*, Progress of Theoretical Physics, 68 (1982), pp. 1827–1840.

[22] E. Peacock-López, D. B. Radov, and C. S. Flesner, *Mixed-mode oscillations in a self-replicating dimerization mechanism*, Biophysical Chemistry, 1997 (1997).

[23] B. Peng, V. Gáspár, and K. Showalter, *False bifurcations in chemical systems: canards*, Philosophical Transactions of the Royal Society A: Mathematical, Physical and Engineering Sciences, 337 (1991), pp. 275–289.

[24] B. Rossetto, *Trajectoires lentes des systèmes dynamique lent-rapides*, in Analysis and optimization of systems, no. 83 in Lecture Notes in Control and Information Sciences, 1986, pp. 680–695.

[25] Antonios Zagaris, C. William Gear, Tasso J. Kaper, and Yannis G. Kevrekidis, *Analysis of the accuracy and convergence of equation-free projection to a slow manifold*, ESAIM: Mathematical Modelling and Numerical Analysis, 43 (2009), pp. 757–784.

[26] A K Zvonkin and M A Shubin, *Non-standard analysis and singular perturbations of ordinary differential equations*, Russian Mathematical Surveys, 39 (1984), pp. 69–131.